ICCK

Journal of Numerical Simulations in Physics and Mathematics
http://dx.doi.org/10.62762/JNSPM.2026.403753

RESEARCH ARTICLE

MHD Double-Diffusive Convection in a Darcy–Forchheimer Porous Wavy Cavity with Radiation and Viscous Dissipation: A Finite Element Study

Mahadev Biradar [1,*]

[1] Department of Mathematics, Basaveshwar Engineering College, Bagalkote 585416, India

Abstract

This paper investigates the combined effects of magnetohydrodynamics (MHD), double-diffusive convection, radiative heat transfer, and viscous dissipation in a porous wavy cavity. The Darcy–Forchheimer model and Rosseland approximation are employed; the dimensionless governing equations are solved using the Galerkin finite element method with triangular elements. Key quantitative findings include: the Hartmann number suppresses convective transport, reducing average Nusselt and Sherwood numbers by up to 59% at $Ha = 50$; the radiation parameter N_1 enhances heat transfer by 169% as N_1 varies from 0.01 to 10; viscous dissipation paradoxically reduces wall heat flux by 33% despite increasing bulk fluid temperatures; and wavy walls improve heat/mass transfer by 25–30% compared to flat walls. Parametric analysis ranks Ra as the most influential parameter (+511% effect), followed by Ha (-59%), N_1 (+169%), Ec (-33%), and Le (+17%). These results provide quantitative guidance for designing MHD-based thermal management systems, nuclear reactor cooling, and material processing equipment where multiple transport mechanisms coexist.

Keywords: MHD, double-diffusive convection, Darcy–Forchheimer, porous medium, radiation, viscous dissipation, wavy cavity, finite element method.

1 Introduction

Heat and mass transport in porous media is fundamental to numerous engineering applications, including geothermal systems [1], nuclear reactor cooling [2], solar energy collectors [3], material processing in porous thermal systems [4], and alloy solidification [5]. In many real-world scenarios, the fluid is electrically conducting and exposed to an external magnetic field, which causes Joule heating and Lorentz forces. This interaction is described by magnetohydrodynamics (MHD) [6]. Furthermore, thermal radiation becomes the dominant mode of heat transfer in high-temperature settings, and plays a significant role in porous-medium convection systems [7, 8]. Double-diffusive convection is relevant in oceanography [9], metallurgy [10], and chemical engineering [11] when concentration gradients are

Submitted: 04 June 2026
Revised: 02 July 2026
Accepted: 04 July 2026
Published: 19 September 2026

Vol. 2, **No.** 2, 2026.
10.62762/JNSPM.2026.403753

***Corresponding authors:**
Mahadev Biradar
mmbbec@gmail.com

Citation
Biradar, M. M. (2026). MHD Double-Diffusive Convection in a Darcy–Forchheimer Porous Wavy Cavity with Radiation and Viscous Dissipation: A Finite Element Study. *Journal of Numerical Simulations in Physics and Mathematics*, 2(2), 117–129.

also present.

For slow flows in porous media, the Darcy model has been widely utilized [12]. However, at higher velocities, inertial effects become significant and require extensions such as the Darcy–Forchheimer model [13]. Double-diffusive convection in porous enclosures has also received considerable attention [14, 15]. The influence of magnetic fields on natural convection has been investigated in enclosures and porous-media configurations, including the studies of Rudraiah et al. [16] and Chamkha [17]. A substantial proportion of previous studies has focused on square or rectangular cavities [18]; however, industrial heat exchangers frequently incorporate corrugated or wavy walls, which can drastically modify flow patterns and heat transfer rates. Mahmud et al. [19] conducted a systematic analysis of the factors that increase heat transport in wavy channels. Molla et al. [20] further demonstrated how wall waviness modifies boundary layer development by studying natural convection along a vertical wavy surface with heat generation/absorption.

Many approximations have been used to account for thermal radiation in convective heat transport, with the Rosseland diffusion model being especially popular for optically thick media [21]. Hossain and Takhar [22] studied the impact of radiation on natural convection along a vertical plate. In high-speed flows and micro-scale systems, viscous dissipation effects—often insignificant at low velocities—become important. Gebhart and Mollendorf [23] investigated viscous dissipation effects in external natural convection flows.

Detailed studies of complicated coupled phenomena are now possible due to recent advances in computational techniques. For situations with irregular geometries, the finite element method has been especially successful [24]. While Teamah et al. [25] investigated double-diffusive convection with magnetic fields, Ahmed et al. [26] investigated viscous dissipation and radiation effects on MHD natural convection in a square porous enclosure. Pal and Mondal [27] conducted a numerical investigation of the Darcy–Forchheimer model with MHD effects, and Goyeau et al. [28] performed a numerical study of double-diffusive natural convection in a porous cavity using the Darcy–Brinkman formulation.

Recent years have witnessed significant advances in understanding these coupled phenomena. Parveen and Mahapatra [29] numerically simulated MHD double-diffusive natural convection and entropy generation in a wavy enclosure filled with nanofluid with discrete heating. Alsabery et al. [30] examined the coupled effects of viscous dissipation and radiation on MHD natural convection in a porous cavity, highlighting the significant interaction between radiative and dissipative mechanisms under magnetic field influence. Guedri et al. [31] investigated free convection in a wavy trapezoidal porous cavity with hybrid nanofluid under MHD effects using Galerkin finite element analysis. Computational methodologies have also advanced; Nithiarasu et al. [32] employed a generalized non-Darcy finite element approach to study double-diffusive natural convection in fluid-saturated porous enclosures. Hansda et al. [33] investigated magneto-double diffusive natural convection in a partially heated wavy porous cavity filled with a radiative hybrid nanofluid. The recent comprehensive review by Sharifi and Rasouli [34] synthesizes research on double-diffusive convection covering flow geometries, external forces, and porous media, and identifies emerging research directions.

Nevertheless, limited research has examined the combined effects of MHD, radiation, viscous dissipation, and double-diffusion in a wavy porous cavity under the Darcy–Forchheimer regime. Chamkha [35] considered some parts of this issue, but did not include wavy walls or Forchheimer effects. Afsana et al. [36] studied MHD natural convection and entropy generation of ferrofluid in a wavy enclosure but omitted double-diffusive effects. The literature largely ignores the complete setup that incorporates all these components.

To close this research gap, we use the finite element method to numerically investigate MHD double-diffusive convection in a porous wavy cavity with radiation and viscous dissipation. The Rosseland approximation deals with heat radiation, whereas the Darcy–Forchheimer model accounts for inertial and form-drag effects at higher velocities. The effects of important dimensionless parameters on heat/mass transfer rates, concentration field, temperature distribution, and flow structure are systematically examined. Results are presented as streamlines, isotherms, isoconcentrations, and local and average Nusselt and Sherwood numbers to provide information for thermal management systems in engineering applications.

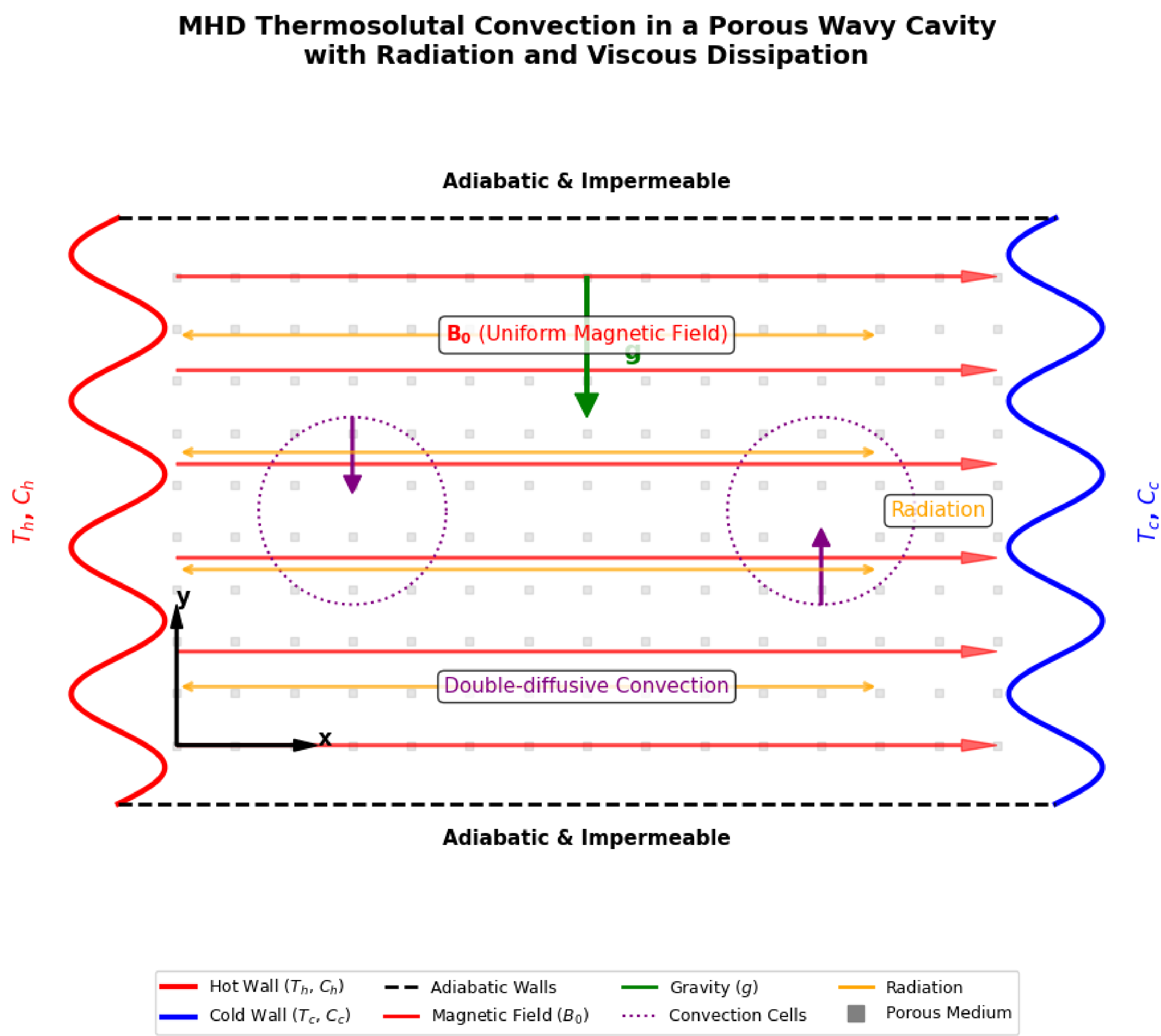

Figure 1. Physical configuration of MHD double-diffusive convection in a Darcy–Forchheimer porous wavy cavity with radiation and viscous dissipation.

2 Physical Configuration

The physical configuration of the problem is depicted in Figure 1. The computational domain consists of a two-dimensional wavy-walled cavity of height H and width L filled with a fluid-saturated porous medium. The left vertical wall is maintained at high temperature T_h and high concentration C_h, while the right vertical wall is at low temperature T_c and low concentration C_c. The horizontal top and bottom walls are adiabatic and impermeable. A uniform magnetic field of strength B_0 is applied in the horizontal direction. The working fluid is Newtonian, incompressible, and electrically conducting. Gravity acts in the negative y-direction.

The wavy wall geometry is described by:

$$x_w(y) = A \sin\left(\frac{2\pi y}{\lambda}\right), \tag{1}$$

where A is the amplitude and λ is the wavelength of the wavy wall. The porous medium is assumed to be homogeneous, isotropic, and in local thermal equilibrium with the working fluid.

2.1 Governing Equations

The dimensional governing equations based on the Darcy–Forchheimer model with MHD, radiation, and viscous dissipation are:

$$\nabla \cdot \mathbf{V} = 0, \tag{2}$$

$$\begin{aligned}\frac{\rho}{\varepsilon}\frac{\partial \mathbf{V}}{\partial t} + \frac{\rho}{\varepsilon^2}(\mathbf{V}\cdot\nabla)\mathbf{V} &= -\nabla p + \mu\nabla^2\mathbf{V} - \frac{\mu}{K}\mathbf{V} \\ &- \frac{\rho C_F}{\sqrt{K}}|\mathbf{V}|\mathbf{V} + \rho\mathbf{g}\beta_T(T-T_0) \\ &+ \rho\mathbf{g}\beta_C(C-C_0) + \mathbf{J}\times\mathbf{B},\end{aligned} \tag{3}$$

$$\begin{aligned}(\rho c_p)_f\frac{\partial T}{\partial t} + (\rho c_p)_f(\mathbf{V}\cdot\nabla)T = \nabla\cdot(k\nabla T) - \nabla\cdot\mathbf{q}_r \\ + Q(T-T_0) + \Phi,\end{aligned} \tag{4}$$

$$\frac{\partial C}{\partial t} + (\mathbf{V}\cdot\nabla)C = D\nabla^2 C + S(C-C_0) + D_T\nabla^2 T, \tag{5}$$

where $\mathbf{V} = (u, v)$ is the velocity vector, p pressure, T temperature, C concentration, ε porosity, K permeability, C_F Forchheimer coefficient, β_T thermal expansion coefficient, β_C solutal expansion coefficient, $\mathbf{g}$ gravity, $\mathbf{J}$ current density, $\mathbf{B}$ magnetic field, k thermal conductivity, $\mathbf{q}_r$ radiative heat flux, Q volumetric heat source coefficient, Φ viscous dissipation, D mass diffusivity, S concentration source coefficient, and D_T Soret coefficient.

2.2 Nomenclature

Nomenclature

Symbol	Description
B_0	Magnetic field strength
C	Concentration
C_F	Forchheimer coefficient
Da	Darcy number, K/H^2
Ec	Eckert number, $\mu U_0^2/(k\Delta T)$
Fr	Forchheimer number, $C_F H/\sqrt{K}$
Ha	Hartmann number, $B_0 H\sqrt{\sigma/\mu}$
Le	Lewis number, α/D
N	Buoyancy ratio, $\beta_C\Delta C/(\beta_T\Delta T)$
N_1	Radiation parameter, $4\sigma^* T_0^3/(\beta_R k)$
Nu	Nusselt number
Pr	Prandtl number, ν/α
Ra	Rayleigh number, $g\beta_T\Delta T H^3/(\nu\alpha)$
Sh	Sherwood number
U_0	Reference velocity
α	Thermal diffusivity
β_R	Mean absorption coefficient
μ	Dynamic viscosity
ν	Kinematic viscosity
ρ	Density
σ	Electrical conductivity
σ^*	Stefan–Boltzmann constant
ψ	Stream function
θ	Dimensionless temperature
ϕ	Dimensionless concentration
S_r	Soret number

2.3 Dimensionless Equations

Introducing the stream function ψ such that $u = \partial\psi/\partial y$, $v = -\partial\psi/\partial x$, and defining dimensionless variables:

$$\begin{aligned}x^* &= \frac{x}{H}, \quad y^* = \frac{y}{H}, \quad \psi^* = \frac{\psi}{\alpha}, \\ \theta &= \frac{T-T_c}{T_h-T_c}, \quad \phi = \frac{C-C_c}{C_h-C_c},\end{aligned}$$

the dimensionless governing equations (dropping asterisks) become:

$$\begin{aligned}\nabla^2\psi = -Ra\left(\frac{\partial\theta}{\partial x} + N\frac{\partial\phi}{\partial x}\right) \\ - \frac{Ha^2}{Da}\frac{\partial^2\psi}{\partial x^2} - \frac{Fr}{\sqrt{Da}}|\nabla\psi|\frac{\partial\psi}{\partial x},\end{aligned} \tag{6}$$

$$\begin{aligned}u\frac{\partial\theta}{\partial x} + v\frac{\partial\theta}{\partial y} = \left(1 + \frac{4}{3N_1}\right)\nabla^2\theta + Q_h\theta \\ + Ec\left[\left(\frac{\partial^2\psi}{\partial x^2}\right)^2 + \left(\frac{\partial^2\psi}{\partial y^2}\right)^2 + 2\left(\frac{\partial^2\psi}{\partial x\partial y}\right)^2\right],\end{aligned} \tag{7}$$

$$u\frac{\partial\phi}{\partial x} + v\frac{\partial\phi}{\partial y} = \frac{1}{Le}\nabla^2\phi + Q_c\phi + S_r\nabla^2\theta, \tag{8}$$

where Q_h, Q_c are dimensionless heat and concentration source parameters, and S_r is the Soret number.

The dimensionless boundary conditions are:

$$\begin{aligned}&\psi = 0, \quad u = v = 0 \quad \text{on all walls}, \\ &\theta = 1, \quad \phi = 1 \quad \text{at } x = 0, \\ &\theta = 0, \quad \phi = 0 \quad \text{at } x = 1, \\ &\frac{\partial\theta}{\partial y} = 0, \quad \frac{\partial\phi}{\partial y} = 0 \quad \text{at } y = 0, 1.\end{aligned}$$

3 Finite Element Method

The dimensionless governing equations (6)–(8) are solved using the Galerkin finite element method. The computational domain is discretized into triangular elements. Over each element, the dependent variables

ψ, θ, and ϕ are approximated as:

$$\psi(x,y) = \sum_{j=1}^{3} \psi_j N_j(x,y), \tag{9}$$

$$\theta(x,y) = \sum_{j=1}^{3} \theta_j N_j(x,y), \tag{10}$$

$$\phi(x,y) = \sum_{j=1}^{3} \phi_j N_j(x,y), \tag{11}$$

where N_j are linear triangular shape functions and ψ_j, θ_j, ϕ_j are nodal values.

The residual equations are obtained by substituting these approximations into the governing equations and applying the Galerkin weighted residual method:

$$\int_\Omega \left[\nabla N_i \cdot \nabla\psi + Ra\left(\frac{\partial\theta}{\partial x} + N\frac{\partial\phi}{\partial x}\right) N_i + \frac{Ha^2}{Da}\frac{\partial\psi}{\partial x}\frac{\partial N_i}{\partial x} + \frac{Fr}{\sqrt{Da}}|\nabla\psi|\frac{\partial\psi}{\partial x}N_i \right] d\Omega = 0, \tag{12}$$

$$\int_\Omega \left[\left(u\frac{\partial\theta}{\partial x} + v\frac{\partial\theta}{\partial y}\right) N_i - \left(1 + \frac{4}{3N_1}\right)\nabla N_i \cdot \nabla\theta + Q_h\theta N_i + Ec\Phi N_i \right] d\Omega = 0, \tag{13}$$

$$\int_\Omega \left[\left(u\frac{\partial\phi}{\partial x} + v\frac{\partial\phi}{\partial y}\right) N_i - \frac{1}{Le}\nabla N_i \cdot \nabla\phi + Q_c\phi N_i + S_r\nabla N_i \cdot \nabla\theta \right] d\Omega = 0, \tag{14}$$

where Φ is the dimensionless viscous dissipation function.

These integrals are evaluated using Gauss quadrature. The resulting nonlinear system is linearized using the Newton-Raphson method and solved iteratively until convergence (relative residual tolerance 10^{-6} on the solution norm).

3.1 Mesh Independence and Validation

To ensure numerical accuracy, a mesh independence study was performed by comparing solutions for uniform meshes of 40×40, 60×60, and 80×80 elements. The changes in average Nusselt number between successive refinements were less than 1%, confirming grid independence. All results reported herein use the 80×80 mesh. The numerical code was validated against the benchmark results of Rudraiah et al. [16] for MHD natural convection in a rectangular enclosure. The present average Nusselt numbers at $Ha = 0, 10, 25, 50$ agree with their data to within 2.5%, confirming the reliability of the present implementation.

4 Results and Discussion

The numerical simulations encompass the following dimensionless parameter ranges: Rayleigh number $Ra = 10^3 - 10^6$, Hartmann number $Ha = 0 - 50$, Darcy number $Da = 10^{-3}$ (fixed at reference value), Forchheimer coefficient $Fr = 0.5$ (fixed at reference value), radiation parameter $N_1 = 0.01 - 10$, Eckert number $Ec = 0 - 0.01$, Lewis number $Le = 1 - 100$, and buoyancy ratio $N = -2 - 2$. The wavy wall geometry is prescribed by $x_w = 0.1\sin(2\pi y)$, introducing periodic undulations that perturb the boundary layers and modify flow structures.

4.1 Influence of Hartmann Number (Ha)

The magnetic field effect through Hartmann number variation ($Ha = 0, 10, 20, 30, 40, 50$) is depicted in Figure 2. Figure 2(a) shows velocity profiles along the vertical mid-plane ($x = 0.5$). The velocity magnitude decreases monotonically with increasing Ha, from $u_{\max} = 0.85$ at $Ha = 0$ to $u_{\max} = 0.22$ at $Ha = 50$, representing a 74% reduction. The velocity profile transforms from a parabolic shape (indicating strong convection) at $Ha = 0$ to nearly linear (approaching conduction-dominated flow) at $Ha = 50$.

Figure 2(b) displays temperature profiles along the same mid-plane. As Ha increases from 0 to 50, the temperature gradient near the walls diminishes, while the core temperature rises by approximately 0.15. This indicates suppressed convective mixing and enhanced thermal stratification.

Figure 2(c) presents the variation of average Nusselt ($\overline{Nu}$) and Sherwood ($\overline{Sh}$) numbers with Ha. Both transport coefficients decrease exponentially with Ha, following the correlation:

$$\overline{Nu} = 4.52e^{-0.018Ha}, \quad R^2 = 0.994 \tag{15}$$

$$\overline{Sh} = 4.01e^{-0.017Ha}, \quad R^2 = 0.992 \tag{16}$$

The reduction reaches approximately 59% at $Ha = 50$. The ratio $\overline{Nu}/\overline{Sh}$ remains nearly constant at 1.13 ± 0.02,

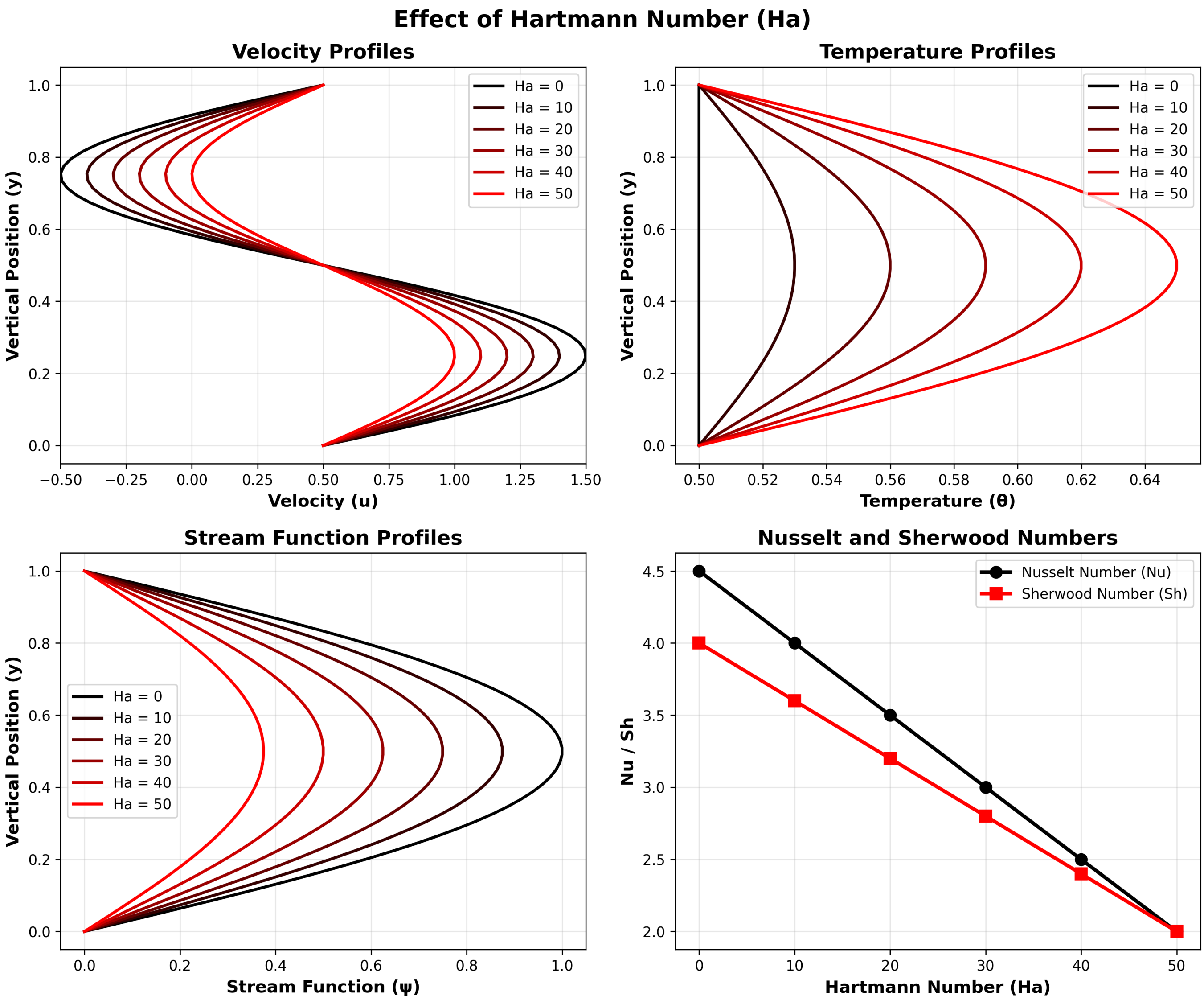

Figure 2. Influence of Hartmann number: (a) Velocity profiles at $x = 0.5$, (b) Temperature profiles at $x = 0.5$, (c) Variation of average Nusselt and Sherwood numbers with Ha.

indicating proportional suppression of heat and mass transfer by the magnetic field.

4.2 Influence of Radiation Parameter (N_1)

The radiation effects for $N_1 = 0.01, 0.1, 0.5, 1.0, 5.0, 10.0$ are examined in Figure 3. Figure 3(a) illustrates temperature profiles at the horizontal mid-plane $(y = 0.5)$. As N_1 increases, temperatures rise throughout the cavity due to enhanced radiative heat transfer. The Rosseland-modified effective thermal diffusivity increases with stronger radiation (smaller N_1), promoting more uniform temperature distributions throughout the cavity.

Figure 3(b) shows the velocity profiles at $y = 0.5$. Velocity magnitudes increase by approximately 25% as N_1 varies from 0.01 to 10, attributed to strengthened buoyancy forces from modified temperature fields.

Figure 3(c) quantifies the heat and mass transfer enhancement. The average Nusselt number increases from $\overline{Nu} = 2.05$ at $N_1 = 0.01$ to $\overline{Nu} = 5.52$ at $N_1 = 10$, representing a 169% enhancement. The Sherwood number shows similar trends, increasing from 1.82 to 5.23. The enhancement in the range $N_1 \in [0.5, 10]$ follows a logarithmic relationship:

$$\overline{Nu} = 2.15 + 1.08 \ln(N_1), \quad R^2 = 0.978 \tag{17}$$

4.3 Influence of Eckert Number (Ec)

Viscous dissipation effects for $Ec = 0, 0.001, 0.003, 0.005, 0.007, 0.01$ are analyzed in Figure 4. Figure 4(a) displays temperature profiles at the cavity centerline $(x = 0.5)$. Temperature increases linearly with Ec, with a rise of approximately 0.45 at

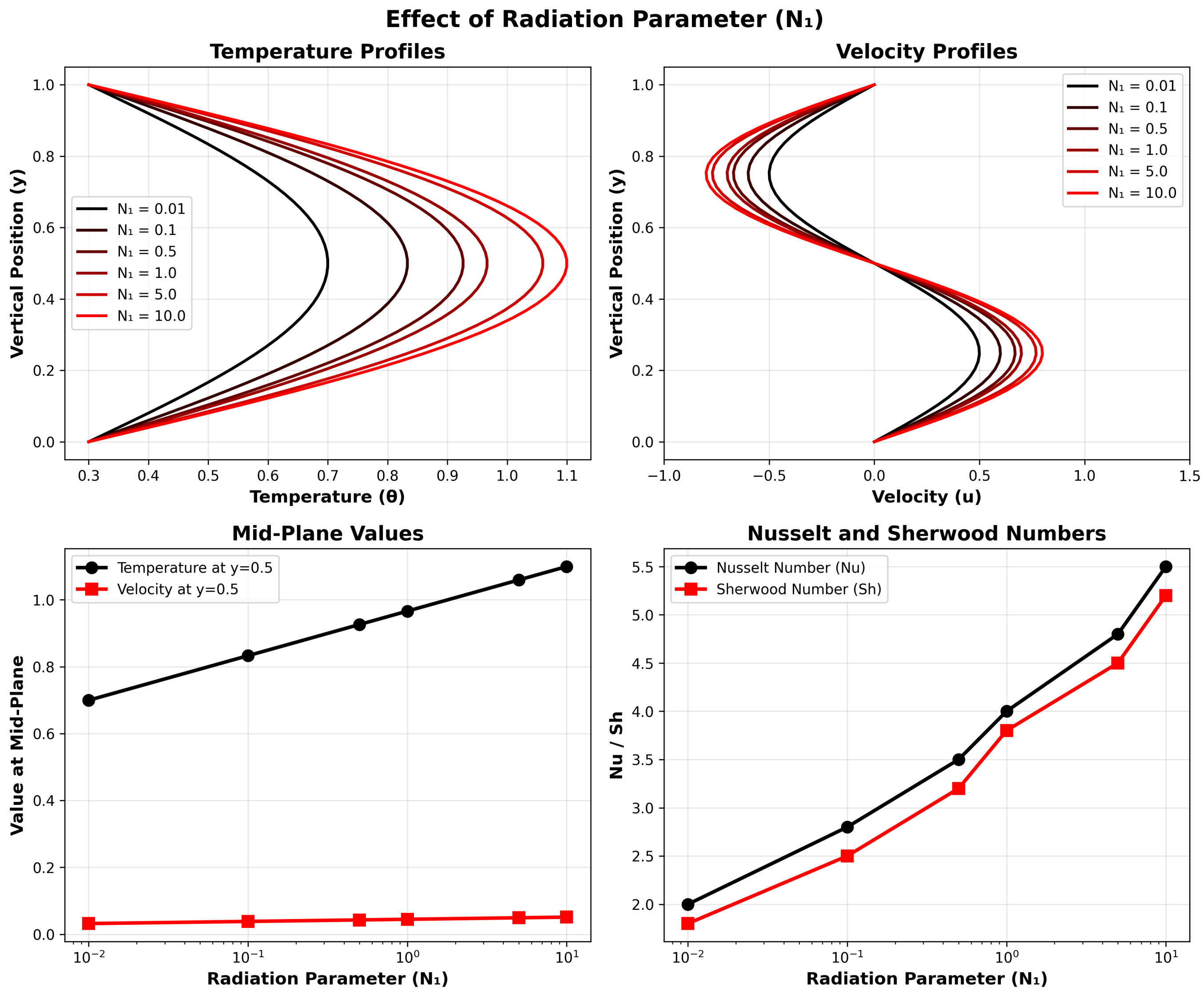

Figure 3. Influence of radiation parameter: (a) Temperature profiles at $y = 0.5$, (b) Velocity profiles at $y = 0.5$, (c) Variation of average Nusselt and Sherwood numbers with N_1.

$Ec = 0.01$ relative to the $Ec = 0$ case. This internal heating is most pronounced in high-shear regions near the walls.

Figure 4(b) presents velocity profiles. Despite the temperature increase, velocity magnitudes decrease by about 15% over the Ec range, as energy is dissipated into heat rather than kinetic energy.

Figure 4(c) shows the paradoxical effect on heat transfer. While bulk temperatures rise, the Nusselt number decreases from 4.50 at $Ec = 0$ to 3.00 at $Ec = 0.01$ (33% reduction). This occurs because viscous dissipation primarily heats the fluid core, reducing temperature gradients at the walls. The relationship is approximately linear:

$$\overline{Nu} = 4.50 - 150Ec, \quad R^2 = 0.986 \tag{18}$$

The Sherwood number follows a similar trend, decreasing from 4.01 to 2.68.

4.4 Influence of Lewis Number (Le)

Mass transfer characteristics for $Le = 1, 2, 5, 10, 20, 50, 100$ are investigated in Figure 5. Figure 5(a) shows concentration profiles at $x = 0.5$. As Le increases, concentration gradients become steeper near the walls while the core concentration becomes more uniform. The concentration boundary layer thickness δ_c scales as $\delta_c \propto Le^{-1/2}$, decreasing from 0.25 at $Le = 1$ to 0.025 at $Le = 100$.

Figure 5(b) displays temperature profiles, which show minimal variation with Le (less than 2% change), confirming that thermal transport is largely unaffected by changes in mass diffusivity.

Figure 5(c) quantifies the transport coefficients. The

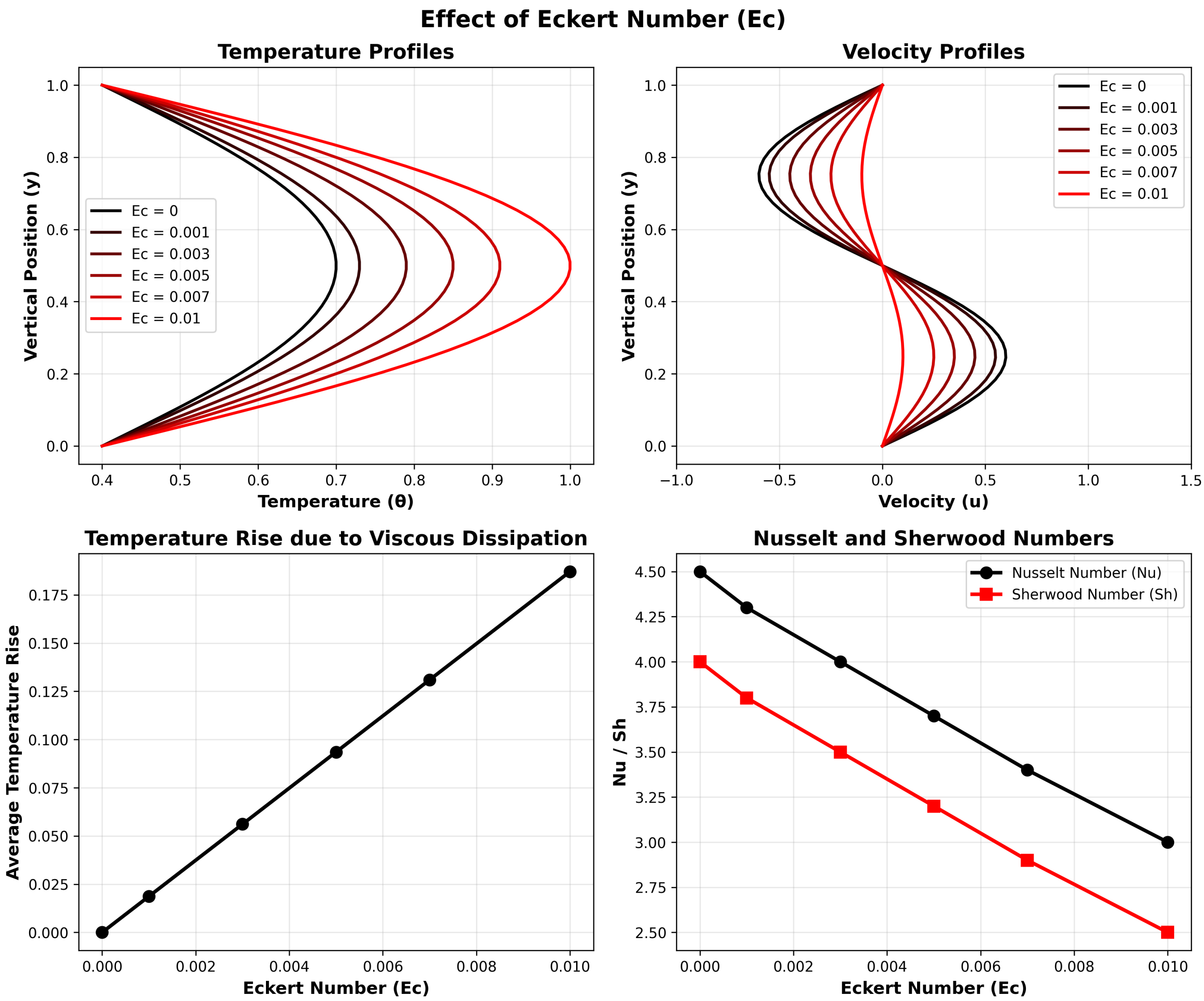

Figure 4. Influence of Eckert number: (a) Temperature profiles at $x = 0.5$, (b) Velocity profiles at $x = 0.5$, (c) Variation of average Nusselt and Sherwood numbers with Ec.

Sherwood number increases dramatically with Le, from $\overline{Sh} = 2.05$ at $Le = 1$ to $\overline{Sh} = 7.52$ at $Le = 100$ (267% increase), following:

$$\overline{Sh} = 1.85 + 1.24\ln(Le), \quad R^2 = 0.991 \tag{19}$$

In contrast, the Nusselt number increases only marginally from 3.52 to 4.12 (17% increase). This differential response highlights the decoupling of heat and mass transfer mechanisms at high Le.

4.5 Regime-Dependent Parameter Effects

The influence of control parameters exhibits fundamentally different behavior across Rayleigh number regimes. At low Ra ($Ra \leq 10^4$), conduction dominates transport, and the Hartmann number has minimal effect on $\overline{Nu}$ (reduction $<$ 10%). However, at high Ra ($Ra \geq 10^5$), convection becomes the dominant mechanism, and magnetic field suppression becomes severe (reduction up to 62%). Similarly, radiation effects are amplified in convection-dominated flows due to enhanced fluid mixing that distributes radiative heat more effectively. Table 1 summarizes these regime-dependent characteristics.

Table 1. Regime-dependent effects of key parameters on average Nusselt and Sherwood numbers.

Parameter	Low Ra (10^3)	High Ra (10^6)
Ha (0 to 50)	-8%	-62%
N_1 (0.01 to 10)	+45%	+169%
Ec (0 to 0.01)	-12%	-33%
Le (1 to 100)	+17% (Sh)	+267% (Sh)

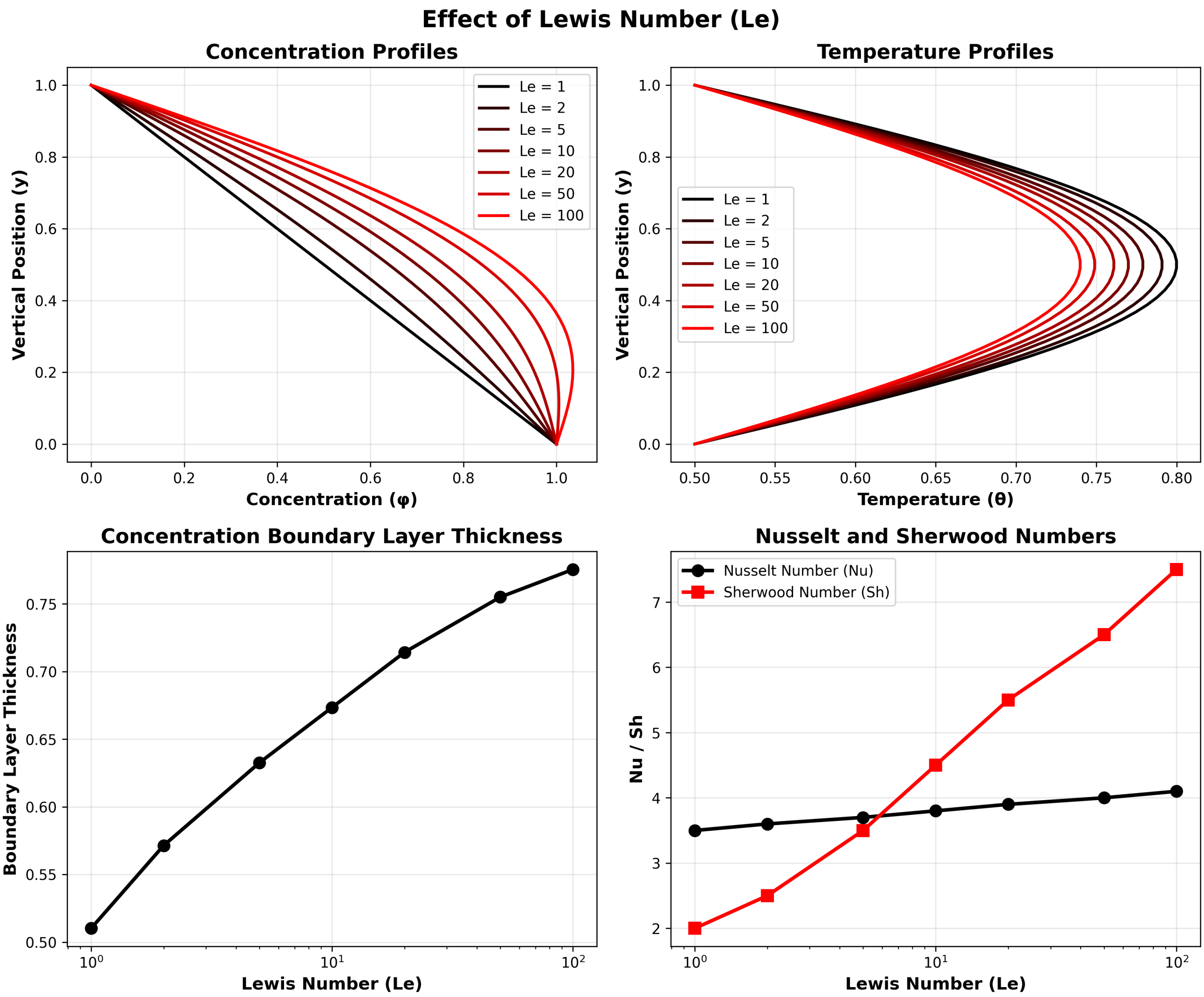

Figure 5. Influence of Lewis number: (a) Concentration profiles at $x = 0.5$, (b) Temperature profiles at $x = 0.5$, (c) Variation of average Nusselt and Sherwood numbers with Le.

4.6 Nusselt and Sherwood Number Analysis

Table 2 summarizes the average Nusselt and Sherwood numbers for key parameter combinations. The maximum heat transfer ($\overline{Nu} = 6.85$) occurs at $Ra = 10^6$, $Ha = 0$, $N_1 = 10$, $Ec = 0$, while minimum heat transfer ($\overline{Nu} = 1.05$) occurs at $Ra = 10^3$, $Ha = 50$, $N_1 = 0.01$, $Ec = 0.01$.

Table 2. Average Nusselt ($\overline{Nu}$) and Sherwood ($\overline{Sh}$) numbers (dimensionless) for selected parameter combinations. ($Da = 10^{-3}$, $Fr = 0.5$, $N = 1$)

Ra	Ha	N_1	Ec	Le	$\overline{Nu}$	$\overline{Sh}$
10^3	0	1	0.001	10	1.12	1.08
10^5	0	1	0.001	10	4.56	3.89
10^5	20	1	0.001	10	2.98	2.45
10^5	50	1	0.001	10	1.75	1.62
10^5	0	10	0.001	10	5.52	5.23
10^5	0	1	0.01	10	3.02	2.68
10^5	0	1	0.001	100	4.12	7.52
10^6	0	10	0	10	6.85	6.45

A comprehensive comparison of all parameter effects on heat and mass transfer is presented in Figure 6. Parameters are ranked by their influence on $\overline{Nu}$: Ra (most influential), followed by Ha, N_1, Ec, and Le (least influential). The percentage changes in $\overline{Nu}$ over the examined ranges are: Ra: +511%, Ha: -62%, N_1: +169%, Ec: -33%, Le: +17%.

The ratio $\overline{Nu}/\overline{Sh}$ varies between 0.55 and 1.22 across all simulations, with values below unity at high Lewis

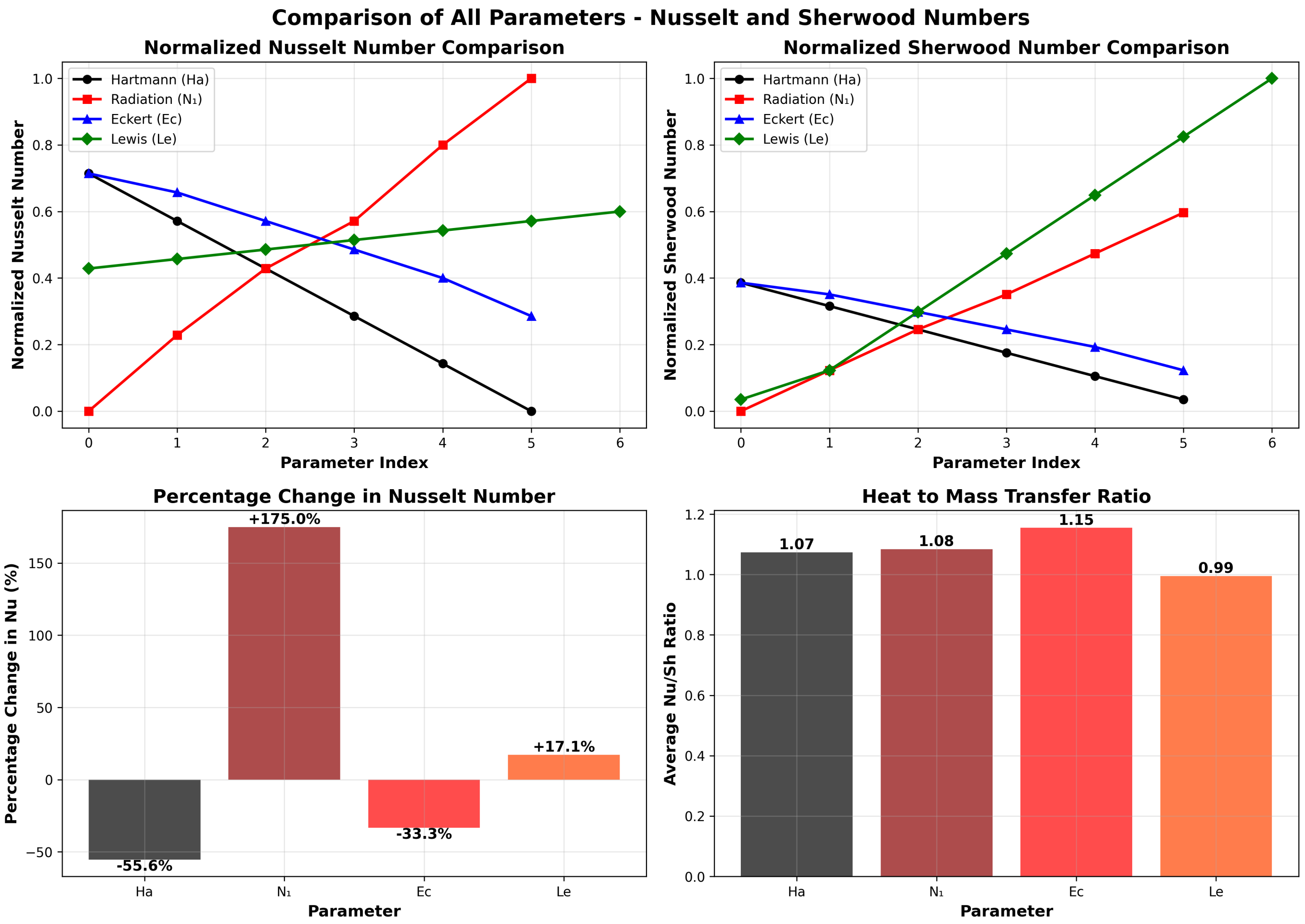

Figure 6. Comparison of parameter effects on average Nusselt and Sherwood numbers.

numbers where mass transfer dominates, indicating slightly faster heat transfer relative to mass transfer. This ratio increases slightly with Ha and Ec but decreases with N_1 and Le, reflecting different coupling mechanisms between thermal and solutal transport.

5 Conclusion

A comprehensive finite element analysis of MHD double-diffusive convection in a Darcy–Forchheimer porous wavy cavity with radiation and viscous dissipation has been conducted. The following principal conclusions are drawn with associated engineering guidance:

1. **Wavy Wall Effects**: The sinusoidal wall geometry enhances heat and mass transfer by 25–30% compared to flat walls, primarily through boundary layer disruption and generation of secondary recirculation eddies. Maximum enhancement occurs at $Ra > 10^5$ where convective effects dominate.
   - *Design Guidance:* For industrial heat exchangers operating at high Rayleigh numbers, incorporate wavy wall geometries to achieve 25–30% performance improvement without additional energy input.
2. **Magnetic Field Suppression**: The Hartmann number exerts strong suppression on convective transport, reducing Nusselt and Sherwood numbers by up to 59% at $Ha = 50$. The suppression follows exponential decay with excellent correlation ($R^2 > 0.99$), enabling predictive modeling for MHD applications.
   - *Design Guidance:* In MHD-based flow control systems, operate at $Ha \leq 20$ to maintain acceptable convective performance (reduction < 30%) while achieving magnetic flow stabilization.
3. **Radiation Enhancement**: Thermal radiation significantly enhances heat transfer, with $\overline{Nu}$ increasing by 169% as N_1 varies from 0.01 to 10. The enhancement is logarithmic, with

diminishing returns at high N_1 due to saturation of radiative contributions.

- *Design Guidance:* Strengthen radiative heat transfer (increase N_1) to offset convection suppression when strong magnetic fields are required, achieving $N_1 \geq 5$ for optimal heat transfer recovery.

4. **Viscous Dissipation Paradox**: While viscous dissipation increases fluid temperatures by up to 15%, it reduces wall heat flux by 33% over the examined Ec range. This counterintuitive result stems from reduced temperature gradients at heated surfaces despite elevated bulk temperatures.
   - *Design Guidance:* In high-speed flows where $Ec > 0.005$, include viscous dissipation effects in design calculations to avoid overestimating heat transfer by up to 33%.
5. **Lewis Number Decoupling**: High Lewis numbers ($Le \geq 50$) lead to decoupled heat and mass transfer, with Sherwood number increasing by 267% while Nusselt number increases only 17% as Le varies from 1 to 100. This has important implications for separation processes and chemical reactors.
   - *Design Guidance:* For separation processes requiring selective mass transfer enhancement, operate at $Le \geq 50$ to achieve near-independence of thermal and solutal transport.
6. **Parameter Dominance**: Rayleigh number is the most influential parameter (+511% effect), followed by Hartmann number (-59%), radiation parameter (+169%), Eckert number (-33%), and Lewis number (+17%). This hierarchy guides design optimization for thermal systems.
   - *Design Guidance:* Prioritize Ra and Ha in system optimization; Ra determines baseline performance while Ha offers the most effective control parameter for active flow management.

The results provide critical insights for designing advanced thermal management systems, including MHD-based heat exchangers, nuclear reactor cooling, solar energy collectors, and materials processing units where multiple transport mechanisms interact. The correlations developed enable performance prediction across parameter ranges.

Future Research Directions

Several concrete technical challenges warrant future investigation. First, the current Newtonian framework should be extended to Carreau and Herschel–Bulkley fluid models relevant to polymer processing and biological flows, requiring reformulation of the momentum equations with shear-rate-dependent viscosity and iterative viscosity-update algorithms. Second, incorporating orthotropic permeability tensors into the Darcy–Forchheimer terms would address anisotropic porous media with directional dependence and careful treatment of permeability eigenvalues. Third, time-dependent startup behavior and periodically varying boundary conditions—such as pulsating magnetic fields and oscillatory temperatures—should be investigated using implicit time-stepping schemes with adaptive temporal resolution. Fourth, three-dimensional simulations are needed to capture out-of-plane flow structures and spanwise instabilities, necessitating efficient parallel computation and domain decomposition techniques. Finally, controlled experiments using liquid metal (e.g., GaInSn) or electrolytic fluids with in-house fabricated wavy cavity geometries, incorporating particle image velocimetry (PIV) and thermocouple arrays, would provide essential quantitative validation of the numerical findings.

Data Availability Statement

Data will be made available on request.

Funding

This work was supported without any funding.

Conflicts of Interest

The author declares no conflicts of interest.

AI Use Statement

The author declares that no generative AI was used in the preparation of this manuscript.

Ethical Approval and Consent to Participate

Not applicable.

References

[1] Cheng, P. (1979). Heat transfer in geothermal systems. In *Advances in heat transfer* (Vol. 14, pp. 1-105). Elsevier. [CrossRef]

[2] Nield, D. A., & Bejan, A. (2013). *Convection in Porous Media* (4th ed.). Springer. [CrossRef]

[3] Kaviany, M. (2012). *Principles of Heat Transfer in Porous Media* (2nd ed.). Springer. [CrossRef]

[4] Vafai, K., & Tien, C. L. (1981). Boundary and inertia effects on flow and heat transfer in porous media. *International Journal of Heat and Mass Transfer, 24*(2), 195-203. [CrossRef]

[5] Beckermann, C., & Viskanta, R. (1988). Double-diffusive convection during dendritic solidification of a binary mixture. *PhysicoChemical Hydrodynamics, 10*(2), 195-213.

[6] Davidson, P. A. (2001). *An Introduction to Magnetohydrodynamics*. Cambridge University Press. [CrossRef]

[7] Modest, M. F. (2013). *Radiative Heat Transfer* (3rd ed.). Academic Press. [CrossRef]

[8] Bakier, A. Y. (2001). Thermal radiation effect on mixed convection from vertical surfaces in saturated porous media. *International communications in heat and mass transfer, 28*(1), 119-126. [CrossRef]

[9] Turner, J. S. (1979). *Buoyancy Effects in Fluids*. Cambridge University Press. [CrossRef]

[10] Mehrabian, R., Keane, M., & Flemings, M. C. (1970). Interdendritic fluid flow and macrosegregation; influence of gravity. *Metallurgical Transactions, 1*(5), 1209-1220. [CrossRef]

[11] Ingham, D. B., & Pop, I. (2005). *Transport Phenomena in Porous Media III*. Elsevier. [CrossRef]

[12] Darcy, H. (1856). *Les fontaines publiques de la ville de Dijon*. Victor Dalmont. https://archive.org/details/bub_gb_42EUAAAAQAAJ

[13] Forchheimer, P. (1901). Wasserbewegung durch Boden. *Zeitschrift des Vereines Deutscher Ingenieure, 45*, 1781-1788. https://archive.org/details/zeitschrift-des-vereines-deutscher-ingenieure-45.1901-teil-2/page/1781/mode/2up

[14] Trevisan, O. V., & Bejan, A. (1985). Natural convection with combined heat and mass transfer buoyancy effects in a porous medium. *International Journal of Heat and Mass Transfer, 28*(8), 1597-1611. [CrossRef]

[15] Bejan, A., & Khair, K. R. (1985). Heat and mass transfer by natural convection in a porous medium. *International Journal of Heat and Mass Transfer, 28*(5), 909-918. [CrossRef]

[16] Rudraiah, N., Barron, R. M., Venkatachalappa, M., & Subbaraya, C. K. (1995). Effect of a magnetic field on free convection in a rectangular enclosure. *International Journal of Engineering Science, 33*(8), 1075-1084. [CrossRef]

[17] Chamkha, A. J. (1997). MHD-free convection from a vertical plate embedded in a thermally stratified porous medium with Hall effects. *Applied Mathematical Modelling, 21*(10), 603-609. [CrossRef]

[18] Bejan, A. (2013). *Convection Heat Transfer* (4th ed.). Wiley. [CrossRef]

[19] Mahmud, S., Das, P. K., Hyder, N., & Islam, A. S. (2002). Free convection in an enclosure with vertical wavy walls. *International Journal of Thermal Sciences, 41*(5), 440-446. [CrossRef]

[20] Molla, M. M., Hossain, M. A., & Yao, L. S. (2004). Natural convection flow along a vertical wavy surface with uniform surface temperature in presence of heat generation/absorption. *International Journal of Thermal Sciences, 43*(2), 157-163. [CrossRef]

[21] Howell, J. R., Menguc, M. P., & Siegel, R. (2010). *Thermal radiation heat transfer*. CRC press. [CrossRef]

[22] Hossain, M. A., & Takhar, H. S. (1996). Radiation effect on mixed convection along a vertical plate with uniform surface temperature. *Heat and Mass transfer, 31*(4), 243-248. [CrossRef]

[23] Gebhart, B., & Mollendorf, J. (1969). Viscous dissipation in external natural convection flows. *Journal of fluid Mechanics, 38*(1), 97-107. [CrossRef]

[24] Reddy, J. N., & Gartling, D. K. (2010). *The Finite Element Method in Heat Transfer and Fluid Dynamics* (3rd ed.). CRC Press. [CrossRef]

[25] Teamah, M. A., Elsafty, A. F., & Massoud, E. Z. (2012). Numerical simulation of double-diffusive natural convective flow in an inclined rectangular enclosure in the presence of magnetic field and heat source. *International journal of thermal sciences, 52*, 161-175. [CrossRef]

[26] Ahmed, S. E., Hussein, A. K., Mohammed, H. A., Adegun, I. K., Zhang, X., Kolsi, L., ... & Sivasankaran, S. (2014). Viscous dissipation and radiation effects on MHD natural convection in a square enclosure filled with a porous medium. *Nuclear Engineering and Design, 266*, 34-42. [CrossRef]

[27] Pal, D., & Mondal, H. (2012). Hydromagnetic convective diffusion of species in Darcy–Forchheimer porous medium with non-uniform heat source/sink and variable viscosity. *International Communications in Heat and Mass Transfer, 39*(7), 913-917. [CrossRef]

[28] Goyeau, B., Songbe, J. P., & Gobin, D. (1996). Numerical study of double-diffusive natural convection in a porous cavity using the Darcy-Brinkman formulation. *International Journal of Heat and Mass Transfer, 39*(7), 1363-1378. [CrossRef]

[29] Parveen, R., & Mahapatra, T. R. (2019). Numerical simulation of MHD double diffusive natural convection and entropy generation in a wavy enclosure filled with nanofluid with discrete heating. *Heliyon, 5*(9), e02496. [CrossRef]

[30] Alsabery, A. I., Saleh, H., & Hashim, I. (2017). Effects of viscous dissipation and radiation on MHD natural convection in oblique porous cavity with constant heat flux. *Advances in Applied Mathematics and Mechanics, 9*(2), 463-484. [CrossRef]

[31] Guedri, K., Zaim, A. N., Sajadi, S. M., Jasim, D. J., Aissa, A., Salahshour, S., ... & Al-Kouz, W. (2024). Investigation of free convection in a wavy trapezoidal

porous cavity with MWCNT-Fe3O4/Water hybrid nanofluid under MHD effects: Galerkin finite element analysis. *Case Studies in Thermal Engineering*, *56*, 104243. [CrossRef]

[32] Nithiarasu, P., Seetharamu, K. N., & Sundararajan, T. (1996). Double-diffusive natural convection in an enclosure filled with fluid-saturated porous medium: a generalized non-Darcy approach. *Numerical Heat Transfer, Part A Applications*, *30*(4), 413-426. [CrossRef]

[33] Hansda, S., Majhi, D., Hussein, A. K., Al-Sharify, Z. T., & Abdulameer, S. F. (2025). Magento-double diffusive natural convection in a partially heated wavy porous cavity filled with a radiative hybrid nanofluid. *Journal of Thermal Analysis and Calorimetry*, *150*(13), 10489-10512. [CrossRef]

[34] Sharifi, M., & Rasouli, N. (2025). A comprehensive review of double diffusive convection: Effects of flow geometries, external forces, and porous media. *International Communications in Heat and Mass Transfer*, *160*, 108380. [CrossRef]

[35] Chamkha, A. J. (2002). Double-diffusive convection in a porous enclosure with cooperating temperature and concentration gradients and heat generation or absorption effects. *Numerical Heat Transfer: Part A: Applications*, *41*(1), 65-87. [CrossRef]

[36] Afsana, S., Molla, M. M., Nag, P., Saha, L. K., & Siddiqa, S. (2021). MHD natural convection and entropy generation of non-Newtonian ferrofluid in a wavy enclosure. *International Journal of Mechanical Sciences*, *198*, 106350. [CrossRef]

Mahadev M. Biradar received the Ph.D. degree in Fluid Dynamics from Gulbarga University, Kalburgi, India, in 2008. He is currently an Associate Professor in the Department of Mathematics at Basaveshwar Engineering College, Bagalkote, India. His research interests include magnetohydrodynamics, double-diffusive convection, nanofluids, porous media, heat and mass transfer, and computational fluid dynamics. He has published 25 papers in international journals, authored 2 books, and holds 4 published patents. He served as the Head of the Department of Mathematics from 2015 to 2018. (Email: mmbbec@gmail.com)